# A hazard-human coupled model (HazardCM) to assess city dynamic exposure to rainfall-triggered natural hazards

Qiang Dai[a, b,*], Xuehong Zhu[a], Lu Zhuo[b, c], Dawei Han[b], Zhenzhen Liu[a], Shuliang Zhang[a]

[a]Key Laboratory of VGE of Ministry of Education, Nanjing Normal University, Nanjing 210023, China

[b]Department of Civil Engineering, University of Bristol, Bristol BS8 1TR, UK

[c]Department of Civil and Structural Engineering, The University of Sheffield, Sheffield S1 3JD, UK

[*]Correspondence: qd_gis@163.com

## Abstract

Human exposure to threats from natural hazards is generally estimated using a static approach with the fixed number of people located in hazard-prone zones; however, in reality this number varies due to population mobility. This study proposes a human–hazard coupled City Model (HazardCM) for accurately calculating city spatiotemporal dynamic exposure to different hazards. It includes four components: an urban environment module, agent-based model, city–hazard coupler, and dynamic exposure assessment. Rainfall-triggered natural hazards under extreme hydrometeorological events were modeled in Lishui, China. Scenarios covering different magnitudes, timings and locations, and return periods of hazards were investigated to derive the spatial distribution and evolution of human exposure. This model is the first that different natural hazards have been analyzed within a unified framework using a dynamic method and offers a new way to investigate exposure's space–time characteristics while considering the dynamic nature of both humans and hazards.

**Keywords:** natural hazards; dynamic exposure; flood; landslide; city model

## 1. Introduction

Natural hazards are growing more intense and frequent in many cities around the world due to the changing climate and anthropogenic activities (du Plessis, 2019). Rising numbers of people in urban areas are becoming increasingly vulnerable to threats from natural hazards. Moreover, natural hazards' negative effects on human society are usually amplified due to the compounding interactions from multi-hazards, such as the concurrence of a storm surge and a flood. There is an urgent need to understand multi-hazards, vulnerability, and risk so as to design more hazard-resilient urban developments.

Both natural hazards and cities can be understood as the systems of systems, and the integration between them is highly complicated. The city itself is an integrated and complex system consisting of heterogeneous and interconnected subsystems pertaining to both physical and social structures, among them humans, infrastructures, organizations, and economy, which are connected by nonlinear, multiple interactions (Atun, 2014). When such a complex system is affected by a hazard, it fails to function as it does in normal conditions due to interrupted interconnections among subsystems. For example, if one water factory is damaged by a hazard, then, owing to the system's interconnectivity, the supply of the electricity (depends on water support) in some urban areas may break down. The challenge lies in understanding how a disruption in a subsystem could affect the whole urban system, for which every detail cannot be foreseen prior to the occurrence of a hazard event (Atun, 2014). In other words, a broad or superficial understanding of the city system as a series of separate components is not enough to be able to comprehend the interactions among subsystems in the city environment.

Just as within a city system, the multi-hazards within an earth system are also complicated. The term "multi-hazards" refers to all possible and relevant hazards and their interactions in a given spatial region and/or temporal period (Gill and Malamud, 2014, 2017; Kappes et al., 2012a). It is often confused with "hazards chain" (or "cascading hazards"), which refers mainly to the interactions among different hazards and the idea that one hazard may induce a series of secondary hazards, also known as the cascading effect, domino effect, knock-on effect, or triggering effect (Kappes et al., 2012b). As the cause–effect relationship does not always exist in the multi-hazards framework, the impact of multi-hazards on city systems is more multifarious. Multi-hazards may be induced by either one kind of driving force or multiple (Gill and Malamud, 2017). Despite relating to a large number of hazards, the multi-hazard structure is relatively simple for a given city. Rain is a significant triggering factor in many hazards, such as landslides, floods, waterlogging, and debris flow. Rainfall-triggered multi-hazards are the most critical issue in many cities (Cho and Chang, 2017).

The analysis of multi-hazards classified by three levels: single-hazard, multi-layer single-hazard, and full multi-hazard model. It is hard to fully understand all hazard mechanisms and dynamic interactions among different hazards, so the full multi-hazard model is still a challenge. On the contrary, the multi-layer single-hazard model, which can provide a detailed model of the mechanisms of each hazard and allow the relationships between different hazards to be examined using a loose coupling approach is a promising way. There are already a large number of mature models for modeling the separate processes of each hazard. For example, the SWMM model has been widely used in many cities to simulate water movement in both urban surface and drainage systems (Bisht et al., 2016; Gironás et al., 2010; Li et al., 2016; Sun et al., 2014). The SHALSTAB model is used to simulate and predict the occurrence of rainfall-triggered landslides (Burton and Bathurst, 1998; Dietrich and Montgomery, 1998; Gorsevski et al., 2006).

The key to assessing the risks of natural hazards is to model the collective consequences of hazards within the city system and human behavior within the multi-hazards environment. The development of an integrated multi-hazards risk assessment model that considers all kinds of hazard interactions together with exposure could offer a way by which city management can reduce risk and increase resilience regarding hazards. Understanding city exposure to natural hazards is one of the most important components of risk assessment. The traditional exposure assessment generally assumes the exposure elements are static and ignores the interactions among these elements (Shabou et al., 2017). Riddell et. al. (2019) considered the dynamics of natural hazards, along with society's exposure and vulnerability; and how these components of disaster risk change over extended periods due to population, economic, climatic drivers, as well as policy and individual decisions for long-term disaster risk reduction. However, as human exposure to a hazard is generally calculated through the number of people located in a hazard-prone zone, this number varies dramatically throughout the day due to population mobility. In an effort to compensate for this variability, “dynamic exposure” (DYE), which refers to the space–time characteristics of exposure, has been defined and applied to flood and earthquake hazards (Hsu et al., 2013; Park and Kwan, 2017; Pittore et al., 2014). Innovations in risk assessment that integrate societal behaviour and behavioural adaptation dynamics into such quantifications may lead to more accurate characterization of risks and improved assessment of the effectiveness of risk-management strategies and investments (Aerts et. al., 2018).However, in a multi-hazards environment, the DYE assessment faces multiple challenges. For example, it is unclear how to define a unified spatial and temporal unit that can be used to model all hazards. Natural hazards are influenced by a range of spatial and temporal scales: from one square meter to one million square kilometers, from a period of seconds to millennia (Gill and Malamud, 2017). Improving the modeled details of one hazard may decrease the computational efficiency of another hazard simulation. Thus, a balance is needed between quality and efficiency for all involved hazards. Furthermore, how to define the exposure elements to different natural hazards and model the hazard processes in a unified platform is also a challenge (Budimir et al., 2014; Mignan et al., 2014; Montz et al., 2017).

To date, there has been little work on simulations of the socioeconomic impact from multi-hazard events and even fewer studies on the dynamic interaction between human behavior and natural hazards (Gill and Malamud, 2017). If a city is susceptible to more than one hazard, better management decisions can be made that will benefit all stakeholders if differential hazard risks, as well as the city's resilience as a whole, can be determined (Atun, 2014). For this reason, this study aims to propose a human–hazard coupled platform for calculating accurate spatiotemporal DYE to different types of natural hazards. Rainfall-triggered natural hazards (including urban floods and landslides) during extreme hydrometeorological events were used for the model, and their DYE was investigated in the context of a typical city in China. People's daily behaviors are characterized by certain patterns with regard to daily, weekly, monthly, and yearly cycles. This study focuses upon daily cycles.

The rest of the paper is organized as follows. Section 2 illustrates the theoretical background of the study. Section 3 describes the structure and components of the model. Section 4 explains the theory of the hazard simulation model. Section 5 presents a case study. Section 6 discusses the results and provides potential improvements of the model. The final section summarizes the key findings and discusses future work.

## 2. Theoretical background

### 2.1 City exposure to hazards

Quantitative natural hazard risk is commonly expressed as a function of the probability of a hazard (P), the exposure to it (E), and the vulnerability of exposed elements (V), which is written as follows (Grahn and Nyberg, 2017):

$$\text{Hazard risk} = P \times E \times V \tag{1}$$

These components can be divided into the hazard event (P) and the actual consequences (E × V) caused by the hazard. In order to perform reliable quantitative risk assessments, it is essential to estimate the values of the three risk components using fine spatial and temporal scales and understand the possible factors that contribute to their change (Grahn and Nyberg, 2017).

Human, building, and infrastructure exposure are crucial inputs for quantitative risk assessment. There are enormous studies to calculate both single and integrated exposure for floods (de Moel et al., 2011; Güneralp et al., 2015; Jongman et al., 2014) and landslides (Garcia et al., 2016; Ivy-Ochs et al., 2009; Pellicani et al., 2014; Promper et al., 2015) in the past decade. However, the dynamic mechanisms relating to hazards and city systems are generally ignored. The impacts of hazards on city systems depend not only on factors such as the magnitude and frequency of the hazard and the exposure of those affected but also on how these variables intersect and evolve in space and time (Terti et al., 2015). For example, the number of people located in hazard-prone zones varies dramatically throughout the day due to the population mobility. A hazard (e.g., earthquake) that occurs during the day surely will have different consequences to one during the night. Moreover, human exposure to hazards depends on how people adapt to changing and potentially dangerous conditions in a specific hazard environment (Terti et al., 2015).

For this reason, DYE that describe the space-time characteristics of exposure is defined and be applied to flood and landslide hazards (Shabou et al., 2017). If human exposure (EH), building exposure (EB), and infrastructure exposure (EI) discretize in terms of space and time, the conceptual form of integrated DYE can be written as follows:

$$E(t, x, y) = EH(t, x, y) + EB(x, y) + EI(x, y), \quad (2)$$

where x and y represent space, and t refers to time of day. The weight and uniformization among these exposure elements are not considered in the conceptual model presented in this study, but they will be considered in the future model versions.

To obtain comprehensive exposure, it is necessary to select representative indicators of every components through expert recommendation or mathematical analysis. The city system was interpreted as a series of blocks in the shape of an irregular polygon. All exposure indicators should be transferred to this unit as well. Uniformization is important because the measurement units of the indicators are not uniform and cannot be directly compared and calculated. Then, according to the characteristics of the indicator data, the weights are determined by expert scoring, analytic hierarchy process and the entropy weight method. Based on the scale table formed by the domain expert's scoring, the weight of the indicators in each criterion layer is calculated according to the analytic hierarchy process, and then the weight of each criterion as well as the combination weight of the indicators are determined.

### 2.2 Human activity and mobility

The location of any given individual with different sociodemographic characteristics varies dramatically over the course of the day (Dawson et al., 2011). As the travel pattern of each individual is generally consistent, it is possible to anticipate his or her location at any given time. The activity-based model microsimulates the variation of an individual's locations by designing the activity planning and scheduling components in a way that it can replicate the individual's actual activity-scheduling behavior (Javanmardi et al., 2016; Rasouli and Timmermans, 2014). It considers travel demand from a human perspective and performs a sequence of activities distributed in space and time (Recker, 1995). Recently, there has been an increasing attention on activity-based models because they can integrate behavioral and psychological factors with the decision-making process (Shabou et al., 2017).

The activity-based model evolved out of the transdisciplinary perspective of time geography, which describes the sequential path of individual events that marks the history of a person within a situational context (Terti et al., 2015). As a complement to this concept, the activity-based model emerged in the 1970s to introduce spatial and temporal constraints on human mobility behavior (Gamow, 1970). McNally (1996) indicated that a qualified activity-based model should have four significant specialties: design travel patterns according to participation demand; simulate by travel sequences instead of an entire trip; connect individual behavior with its sociodemographic characteristics; and consider travel-activity constraints using spatial, temporal, and interpersonal factors (Shabou et al., 2017). Activity-based models attempt to accurately predict how, why, when, how often, where, and with whom a sequences of activities are carried out by individuals at different times of the day and across the days of the week (Bhat and Koppelman, 1999). As the necessity for modeling activity scheduling has become more evident, various operational models have been developed over recent years, including SCHEDULER (Gärling et al., 1994), TRANSIMS (Smith et al., 1995), TASHA (Miller and Roorda, 2003), CEMDAP (Bhat et al., 2004), ALBATROSS (Arentze and Timmermans, 2000), MATSim (Balmer et al., 2006), and ADAPTS

(Auld and Mohammadian, 2012). All these models include the abovementioned four specialties and the same activity-based paradigm. The ADAPTS model was adopted in this study, as it provides a comprehensive modeling method for activities outside the home.

### 2.3 Human adaptation to hazard evolution

Humans' behavior when facing a life-threatening event (such as a natural hazard) is a complicated process and can be driven by many factors. Crisis circumstances and individual sociodemographic characteristics are two basic conditions that determine human adaptation to hazards evolution (Dawson et al., 2011; Terti et al., 2015). Crisis circumstances include the hazard environment (e.g., flood depth, spatial extent of an inundation, and sediment volume of a landslide) and hazard-induced disturbances (e.g., traffic jam or the collapse of an old building). Sociodemographic characteristics, meanwhile, are classified by general (e.g., age, education, and occupation) and hazard-related features (e.g., previous hazard experience and emergency training). One's perception of crisis circumstances and their cues (such as official warning messages) strongly depend on an individual's sociodemographic characteristics. Information diffusion and social interactions that allow people to connect with their relatives and promote a group response are also considered in the published literature (Lindell and Perry, 2003; Ruin et al., 2014). In addition, as an individual adaptation to hazards is governed by a set of institutional rules, institutional analysis has been introduced to model social memory (e.g., social awareness of hazard risk) and impact on individual status (Abebe et al., 2019; David et al., 2017).

The nature and dynamics of an individuals' adaptation to a hazard will differ according to the location and activity they were conducting when they perceived the crisis circumstances (Terti et al., 2015). For example, when a hazard-caused disturbance occurs in the context of an individuals' daily route, his or her familiarity with the surrounding environment may help him or her determine an alternative, safer route, and thus positive actions may be easily adopted. However, an individual's activities may not be easily changed in some special situations, such as picking up a child from school.

## 3. The proposed HazardCM

### 3.1 Model structure

This study proposes a human–hazard coupled city model to describe the impact of rainfall-related hazard events on socioeconomic factors within an agent-based framework with a specific reference to the dynamics of the hazards and the human environment. The framework of the proposed city model is shown in Figure 1. It starts with city elements related to natural hazards by first modeling blocks and networks. HazardCM regards the city as a combination of a series of spatialized irregular blocks connected by various networks (such as road and electricity). A large number of agents are then generated representing different agent types (citizen and government) and population variability. The behaviors, with special consideration for hazard adaptation, and decisions of these agents are predefined. The daily activity and location of citizen agents, from which needs (e.g., water needs), environment impact (e.g., wastewater), and hazard interaction emerge, are simulated. Based on the agent modeling, the hazard processes are carried out using open-source, widely-recognized models, and the hazard consequences are simulated through GIS spatial analysis packages, together with network analysis by Network X (Hagberg et al., 2008) and graph theory (West, 1996). Finally, the spatially and temporally distributed data of rain events are used to drive multiple hazard events, and the corresponding hazards exposure is calculated.

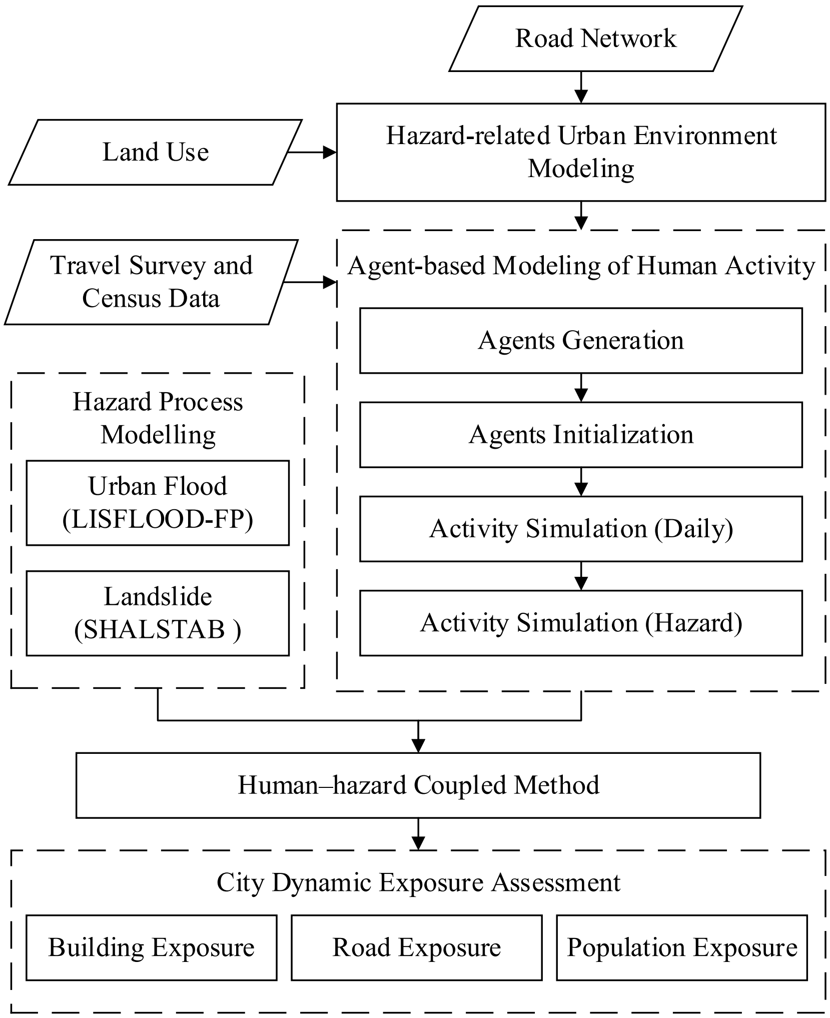


Figure 1. Model structure.

HazardCM follows the concept of InaSAFE (2014), which combines one exposure data layer (e.g., location of buildings) with one hazard scenario (e.g., the footprint of a flood) and returns a spatial impact layer along with a statistical summary and action questions. The socioeconomic process simulation in HazardCM benefits greatly from the resilience.io model (Triantafyllidis et al., 2018), which aims to build a more resilient city by assessing infrastructure design and effectiveness in meeting growing resource demands through integrating a set of models of infrastructure systems within a socioeconomic context. HazardCM is also inspired by WaterMet$^2$ (Behzadian et al., 2014) and RepastCity (2012) in modeling the urban water and traffic systems and Repast Simphony (2016) and Netlogo (2018) in defining the agents and behaviors.

The model components follow a sequentially implemented mechanism, which includes:

(1) hazard-related city elements modeling that provides spatial and feature expressions of the geographical entities of the city (see Section 3.2);

(2) agent-based modeling (ABM) as the simulation module that estimates the population's spatial and temporal distribution and its change (see Section 3.3);

(3) a human–hazard coupled module that reconstruct the simulated hazard elements to adapt to the city system framework (see Section 3.4); and

(4) a DYE calculation as the simulation module that systematically combines the hazard and human evolution processes with respect to the usefulness of these processes in order to quantify the consequences of rainfall-related hazards (see Section 3.5).

The model can be driven by different configurations of hazards and city systems to derive the spatial distribution and evolution of human exposure. The detailed description of the scenario design is given in Section 5.5.

### 3.2 Hazard-related urban environment modeling

Due to the complexity of a city, its geographical entities such as buildings, bridges, and lawns cannot be modeled individually. Instead, HazardCM divides the city into a series of blocks according to land use and road networks. If the discretization is carried out on different spatial scales, the result is multiple resolutions of blocks. With higher spatial resolutions, more details of the city can be identified but at the cost of computational efficiency.

For each block, the input–output flow (water, energy, and waste) moves through networks that allow resources to import and export. Four types of input–output flows are considered in HazardCM: water, wastewater, electricity, and gas. Considering the limited damage of the hazards used in this study (flood and landslides) on resource flow, the network damage from hazards is ignored. The key network nodes (such as water plants and electrical substations) are considered to monitor the input and output flow function for each block.

In the HazardCM model, blocks are classified based on land use, and most are recognized as either Residence, Business, or Recreation, indicating the most important commutes of citizens within a day. Other city elements are classified into these three types as well, for example, a restaurant is considered as a Business block if it covers a large area or is merged with a Resident block if it only occupies some floors of a residential building. As exceptions, chemical-related and public-related blocks are classified separately due to their potential risks/impacts. The chemical-related blocks include printing offices, petroleum, pharmaceutical, and plastics factories. Damage to such blocks may result in serious environmental impacts. Although a pollutant diffusion model is not included in HazardCM, the chemical-related blocks will be highlighted and tracked as a hazard event progresses. Public-related blocks include fire stations, police stations, water plants, power plants, schools, and hospitals. Damage to these blocks may cause breakdowns of public services and subsequent damage to the whole city system. In other words, consequences from a given hazard may transfer from one block to another because of their interconnected nature.

Based on the aforementioned facts, it is necessary to consider elements that may be at a greater risk of failure because of their physical, geographical, cyber, or logical connections in the city system. To model these connections, HazardCM uses the graph theory to simulate the virtual connections among different blocks and uses the correlation matrix (CM) to describe the subsistent network. The virtual connection indicates the unseen interconnections among different elements, such as hospitals and residents. To fully understand the city system's exposure to a hazard, it is necessary not only to represent but also to quantify these interconnections. A graph G = (N,L) consists of two sets of N (nodes) and L (links): the nodes represent a single block exposed to a hazard, while the links represent the interaction among the blocks. HazardCM focuses on building the graph network for public-related blocks. It assumes that all households choose or are assigned public services in the geographical area nearest to them. Such an assumption is applicable for most types of public services, such as police and fire stations, but cannot be used for some self-selecting public-related blocks. For example, theoretically speaking, it is possible for a child to choose any school rather than the one nearest to him or her within a city. However, the disturbance caused by such exceptions is acceptable as we are interested in modeling the generalized relationship among city elements on a large scale instead of accurately simulating it for each individual person.

The subsistent network represents the transit resources (such as water and electricity) among different blocks. The connectivity between two blocks is expressed as a positive number or zero in the CM. The stroke model (Li and Dong, 2010; Porta et al., 2006) is used to generalize the subsistent network. The stroke technique concatenates separate line segments (e.g., conduits) into longer lines to detect and resolve spatial inconsistencies; this provides a more integrated structure to further improve the efficiency of subsequent processing (Li and Dong, 2010). As the model focuses on the connectivity among different blocks, dynamic flow simulation is not carried out in the model.

One of the most important factors of each block is the population within it. As people can travel among different blocks and are affected by the environment, the population changes with time. A detailed description regarding the simulation of the spatial and temporal distribution of the population and its relationship to the hazard's progression is given in the following section.

### 3.3 Agent-based modeling of human activity

ABM uses a type of computational model that can simulate the actions and interactions of autonomous agents in order to assess their effects on the system (House-Peters and Chang, 2011). The ABM of human activity established in this study included agents and daily routine maps. The agent represents a single person or group of people in HazardCM. Some details about agents and their attributes are shown in Table 1. In the ABM, the first step is to generate a sample of agents. A master table, which contains approximately 1,000 agents per block using 12 combinations of characteristics, as per Table 1, is used by the ABM to draw a random sample of agents for the simulation. The sample number is a balance between efficiency and quality, and the number 1,000 was chosen for the study area by a series of experiments. The final simulation outcome based on these agents is scaled up according to their proportion of the population to obtain results for the whole population.

**Table 1:** Agent type.

| Variables | Values |
|---|---|
| Gender | Male/Female |
| Age | 0-17/18-60/60+ |
| Professional status | Employed/Not active or unemployed |
| Education Level(Highest diploma) | University, school-college, bachelor/No diploma |
| Travel mode | Walk/Bus/Car |

The second step involves all agents beginning at their respective home blocks to begin the model scenario. Each agent either stays in a building or moves through the model domain along the road network from a start block to a target block. The choice and time of the journey are defined by the daily routine map as described earlier. The locations of agents are tracked, and the population of each block is aggregated at each time step.

The third step is to run the agent activity-based model, which simulates the agents' locations that vary over the course of the day. As discussed in Section 2.2, the activity-based model represents the processes related to the daily mobility and sequence of human activities including where agents are (e.g., inside a building, on the road) and what they are doing (e.g., studying, working) at different times of the day and across the days of the week (Terti et al., 2015). The daily routine map is defined in HazardCM to guide the behavior of citizen agents. In the daily routine map, each agent is described using a probabilistic finite state machine that describes his or her possible states, the actions he or she can take, and the transitions between states. A similar method was used in Dawson et al. (2011) and Terti et al. (2015). An example of a synthetic daily routine map for an agent with demographic properties is shown in Figure 2.

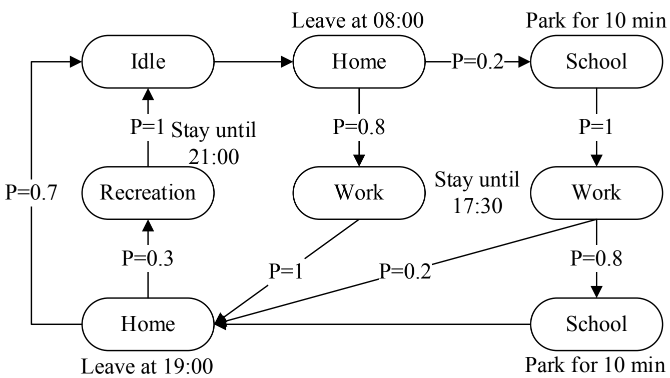


Figure 2. Example of daily activity behaviour map for an employed male agent aged 18–60 years. In this example daily routine map, the agent starts the day at 8 am on weekdays. There is a 0.8 probability that he will go straight to work, going home, and so on. The detailed daily routine map generated from travel survey and census data is given in Section 5.3.

In addition, human behavior during the hazard event is determined by the coincidence of the hazard event with the individual's daily scheduled activities (Terti et al., 2015). The agent will take action under three kinds of situations: perception of environmental cues (e.g., heavy rain), perception of hazard (e.g., water depth and velocity exceed a certain threshold at the agent's location) and receiving of warning messages. The nature and dynamics of the agent's adaptations will differ according to the location and activity he or she was performing when he or she felt the need for action (Ruin et al., 2014; Terti et al., 2015). If the agent perceives a threat, he or she will choose to take an action with a predetermined probability, otherwise he or she will continue the routine as normal. The reaction is achieved by defining different daily routine maps for each hazard adaptation. For example, the daily routine maps for bad weather and warning scenarios are shown in Figure 3. The "bad weather" scenario was similar to the "daily activity" pattern. For instance, the change in travel probability during "bad weather" due to a rainstorm reflected the adaptive behavior of residents. The "warning" scenario assumed that the government had issued early warning information at 08:00 LT, that schools had suspended classes on weekdays, and that the resident responses were stronger than those to the "bad weather" scenario, thereby resulting in a greater difference in activity patterns.

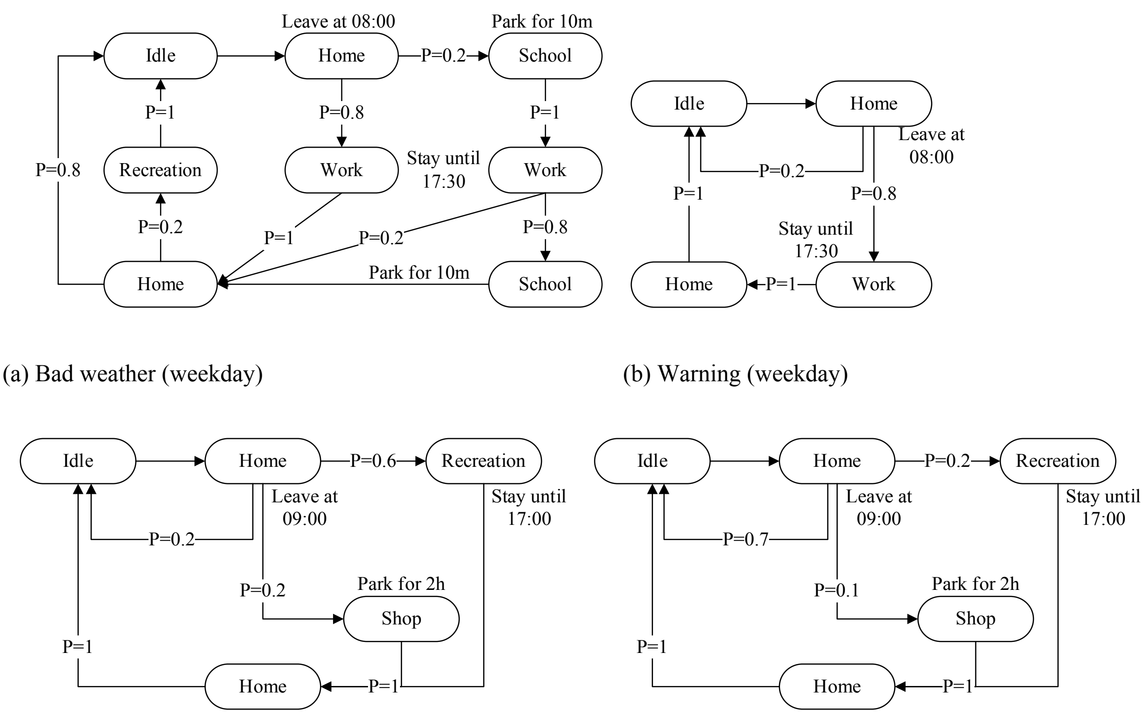


(a) Bad weather (weekday) (b) Warning (weekday)

(c) Bad weather (weekend) (d) Warning (weekend)

Figure 3. Daily routine maps for bad weather and warning scenarios.

It is worth mentioning that the ABM includes some basic assumptions. For example, human daily activity follows a fixed and periodic scheme. Daily periodic activity is assumed to be fixed. However, strictly speaking, the location of most people within the city at a given time is conditional and random, especially at the dividing point where location changes. In addition, only citizens within the city are considered in HazardCM while the incoming and outgoing population is ignored.

### 3.4 Human–hazard coupled method

In HazardCM, the hazard process is coupled with the city system externally or internally depending on the complexity of the hazard's evolution. The external coupled method independently simulates the hazard process and couples it with HazardCM through a dynamic link library, while the internal coupled method is coded inside HazardCM and directly communicates with other functions. The internal method is certainly more efficient, but it is difficult to interpret and implement all hazard-related physical processes. Considering HazardCM aims to couple with various kinds of hazards, the external coupler with a mature hazard simulation model is more practical for our purposes.

The city system is interpreted as a series of blocks in the shape of an irregular polygon. The output of the hazard model should be transferred to this unit as well. Two kinds of transformations are supported in HazardCM: polygon to polygon and raster to polygon. The GIS spatial analysis packages were adopted to implement these transformations. A topological relation is first established to construct the spatial connection between model output units and city blocks. All output values contained in a city block are then summarized by averaging, counting, maximizing, and the like.

### 3.5 City dynamic exposure assessment

In traditional exposure assessments, the city elements layer (e.g., buildings and population) is overlaid with the hazard footprint to obtain a direct exposure layer that represents the direct impact of a hazard on the city system. Based on the simulated results of the hazard's evolution and human activity, HazardCM investigates the city's dynamic and systematic exposure to the hazard. The DYE reveals the dynamic characteristics of the city elements while considering people's mobility and adaptation actions when faced with hazards.

The exposure and hazard variables have to be predefined in the model. In HazardCM, buildings (different types), roads, and population are the three major exposure variables. Special attention is paid to the road network as it links the city elements and transfers hazard consequences from one block to others and is often disrupted due to natural hazard events. Population exposure indicates the population affected by the hazard. People on the road are particularly exposed to road hazards (such as flooding) during their daily mobility (Shabou et al., 2017).

In terms of hazard variables, there are different combinations of indicators for different hazards. Taking flooding as an example, Figueiredo et al. (2018) listed all the hazard variables in current publications and found that water depth, flow velocity, inundation duration, contamination, and return period have been used. For landslides, indicators such as sediment volume and depth can be used as hazard variables. Considering the hazard simulation model used in this study, both water depth and velocity were used to determine flood exposure, while the occurrence of landslides was used as the landslide variable. The selection of variable threshold is discussed in Section 5.3.

# 4. Hazard process modeling

## 4.1 Urban flood modeling

The two-dimensional hydrodynamic model LISFLOOD-FP (Bates and De Roo, 2000) can be used to simulate the evolution of a flooding event. The hazard simulation process is coupled with the city system using the external coupled method. LISFLOOD-FP, developed at the University of Bristol, integrates a one-dimensional river hydraulic movement and a two-dimensional floodplain water movement based on a raster grid. Since the model was published in 2000, it has been widely used around the world and has been proven to simulate properly flood inundation for fluvial, coastal, and urban events (Coulthard et al., 2013; Wood et al., 2016; Lant et. Al., 2010; Ozdemir et. Al., 2013).

LISFLOOD-FP assumes that the flow between two cells is simply a function of the free surface height difference between those cells (Bates and De Roo, 2000):

$$\frac{dh^{i,j}}{dt} = \frac{Q_x^{i-1,j} - Q_x^{i,j} + Q_y^{i,j-1} - Q_y^{i,j}}{\Delta x \Delta y} \tag{3}$$

$$Q_x^{i,j} = \frac{h_{flow}^{5/3}}{n}\left(\frac{h^{i-1,j} - h^{i,j}}{\Delta x}\right)^{1/2} \Delta y \tag{4}$$

where $h^{i,j}$ is the water free surface height at the node (i,j); $\Delta x$ and $\Delta y$ are the cell dimensions; $n$ is the effective grid scale Manning's friction coefficient for the floodplain; and $Q_x$ and $Q_y$ describe the volumetric flow rates between floodplain cells in $x$ and $y$ directions. The flow depth, $h_{flow}$, represents the depth through which water can flow between two cells, and $d$ is defined as the difference between the highest water-free surface in the two cells and the highest bed elevation. The detailed description of LISFLOOD-FP can be found in Bates et al. (2013).

## 4.2 Landslide modeling

The simple, open-source model SHALSTAB is introduced in HazardCM for landslide modeling (Montgomery and Dietrich, 1994). SHALSTAB is a physically-based model designed for identifying areas susceptible to rainfall-triggered shallow landslides on a hydrological catchment scale. The model started as a digital terrain model for mapping the pattern of potential shallow slope instability by building upon the hydrological model TOPOG (O'loughlin, 1986). The slope stability component uses the relative soil saturation to analyze the stability of each topographic element for the case of cohesionless soils of spatially constant thickness and saturated conductivity (Montgomery and Dietrich, 1994).

The model output constitutes landslide susceptibility and critical rainfall. Landslide susceptibility ranges from 1 to 7, and the specific meaning of each value is shown in Table 2. For example, the value 2 indicates that the area is prone to landslides under the rainfall of 0 mm▪day$^{-1}$ to 30 mm▪day$^{-1}$ (critical rainfall).

**Table 2:** The meaning of different landslide susceptibility values.

| Landslide susceptibility value | Critical rainfall (mm/day) |
|---|---|
| 1 | Unconditionally Unstable |
| 2 | 0-30 |
| 3 | 31-100 |
| 4 | 101-150 |
| 5 | 151-200 |
| 6 | 201-999 |
| 7 | Stable |

There are of course more complicated models that describe the mechanism of the landslide process. However, SHALSTAB can be used as an approximation of the surficial mechanics controlling slope stability (Dietrich and Montgomery, 1998). It is implemented as an internal coupled method in HazardCM.

# 5. Case study

## 5.1 Software implementation

The model was implemented in Visual Studio Code and Python programming language using simulation libraries including Qt, Geopandas, and Matplotlib. A series of different software tools were used in the making of this model: QGIS (2018) to provide spatial analysis packages; Network

X (Hagberg et al., 2008) to analyze the traffic routines of citizen agents; and YAML (2017) for data serialization of model input–output.

### 5.2 Data analysis and pre-processing

The city of Lishui in Zhejiang Province, China, was chosen as the area for pilot-testing the model. The center of Lishui is relatively flat and surrounded by mountains, with the Oujiang River running across its southern and eastern areas (see Figure 4). During the flooding period in May and June, the frequency of heavy rainstorms and persistent concentrated rainfall events rise remarkably, raising the probability of floods and landslides. The study area mainly covers the central district of Lishui with an area of 43.4 km$^2$ and has a population of about 71,673 (see Figure 4).

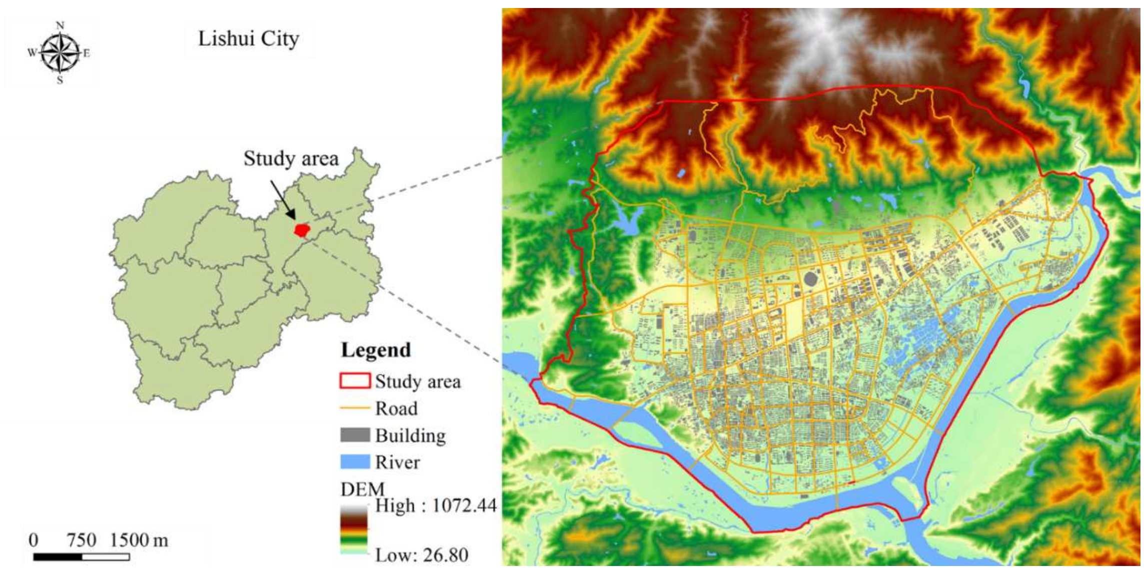


Figure 4. Map of the study area.

**Table 3:** Description of the data used.

| Data | Source | Date | Use |
|---|---|---|---|
| Digital elevation model | Local government | 2013 | Topography |
| Basic geographic data | Local government | 2015 | Location of river and building |
| Chemical points | Local government | 2018 | Location |
| Network data | Local government | 2015 | Location of rainwater, wastewater, water supply, electricity, gas and road networks. |
| 1 km grid population data | National Earth System Science Data Sharing Infrastructure, National Science & Technology Infrastructure of China (http://www.geodata.cn) | 2010 | Number of residents in grid of the study area. |

| | | | |
|---|---|---|---|
| Population profile | Lishui Statistical Yearbook and Liandu Yearbook (http://tjj.lishui.gov.cn) | 2014 | Gender profile, age profile, education level profile, employment profile and travel mode profile. |
| Traffic flow data | Local government | June 2017 -July 2017 | Number of vehicles passing through traffic intersections within one hour. |
| Historical hazards survey | Local government (http://www.zjjs.com.cn) | 2014 | Location and time of historical hazards |

The environmental data to support both flood and landslide simulation and the socioeconomic data to drive the ABM were collected for the study area. The descriptions and sources of the major data used are listed in Table 3. The data were pre-proceed to unify the coordinate system, extent, and scale. To conduct the model parameterization, census data were obtained from the local survey department.

The rainwater, wastewater, water supply, electricity, gas, and road networks are shown in Figure 5. Only newly built communities in Lishui have a gas pipeline network.

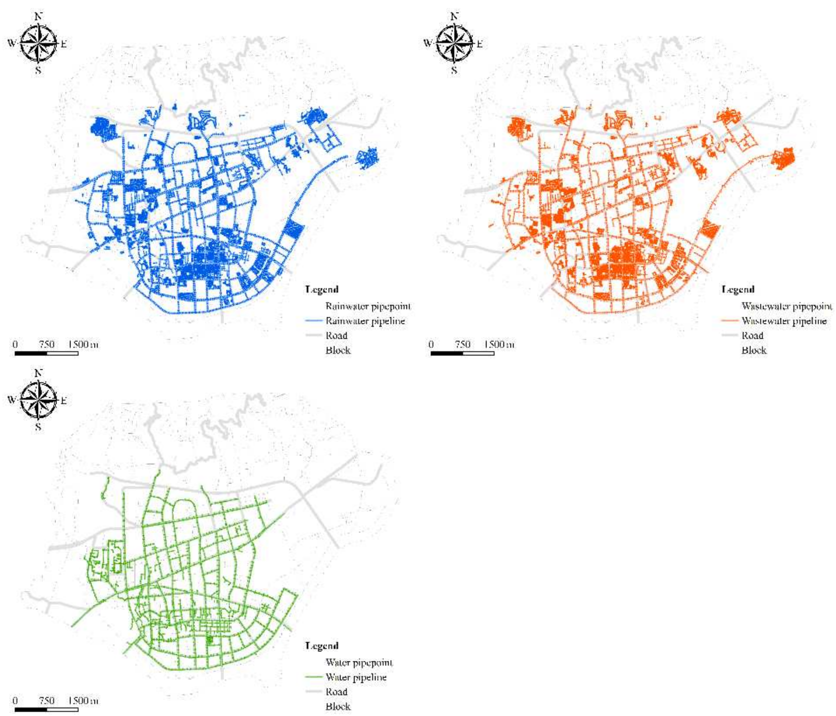


(a) Rainwater network (b) Wastewater network (c) Water supply network

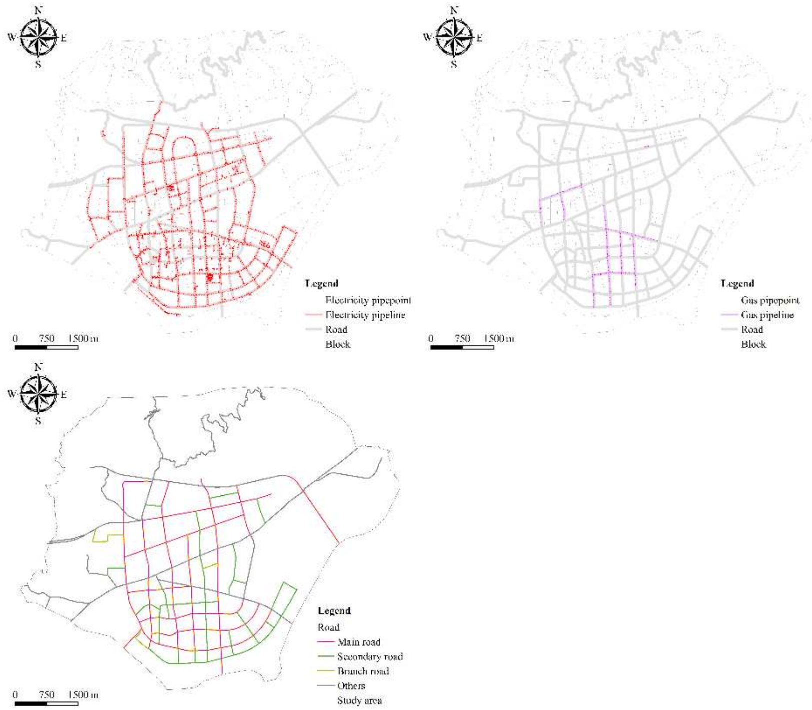


(d) Electricity network (e) Gas network (f) Road network

Figure 5. Map of the networks.

### 5.3 Initial conditions and parameter calibration

HazardCM organizes the city with a series of blocks connected by a variety of networks. According to land use data, the study area was divided into 293 blocks (see Figure 6). The blocks were classified by residence, business, recreation (e.g., shopping center, museum, tourist attraction, and park), public services (e.g., school, hospital, fire station, police station, power plants, and water plants) and others (e.g., river). Chemical type was not shown since the data was point type. The mountains were classified as recreation blocks (for travel), locating on the northern and eastern sides of the study area. The resident blocks are surrounded by mountains and the river dominate the study area.

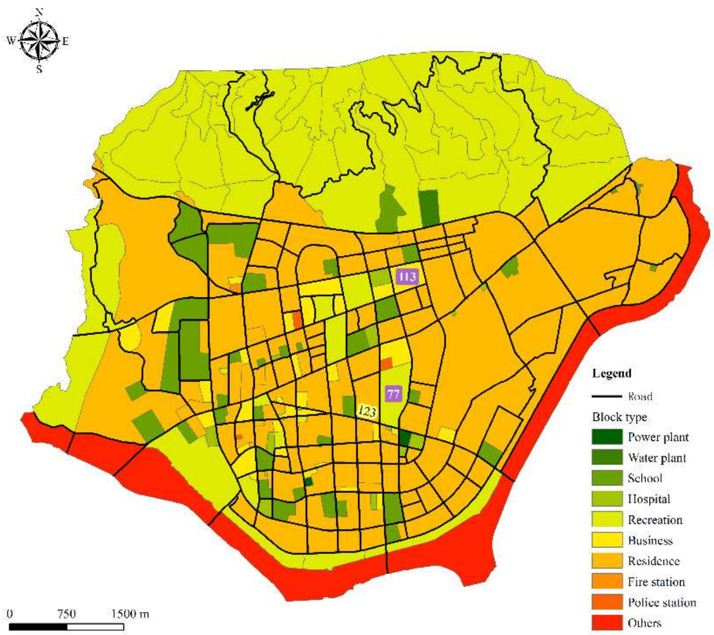


Figure 6. Map of blocks.

The complex and intricate networks were generalized based on their capacity and structure. The original dense network was represented by a simpler network, where their connection nodes were set at the center of blocks. In the programming, the network connection was expressed with a two-dimensional matrix. There may be a degree of loss with this generalization. For example, the original multiple connections between two blocks were simplified into one. However, the model is most concerned with connections among different blocks.

There are two components driving the agent-based model: how the citizen agents behave under normal situations that determine where they are at different times of the day and how agents respond to a hazard event, or adaptation measures. Based on the local survey, sample logs of travel patterns for different agent types were generated (see Figures 2 and 3). The probability of being in a state was also parameterized using the proportion of journeys in each travel pattern, thus producing the daily activity behavior parameters. At the start of the HazardCM model, the agent population was generated and randomly located within residential blocks. The total number of human agents was set to 71,673 by balancing the computation efficiency and representation. The time 00 am was chosen as the start time of the model for all events because most people are at home at this time. The time step iteration was set to 30 minutes, which means the status (including location) of agents changes every 30 minutes.

For the LISFLOOD-FP and SHALSTAB simulations, the grid size was set to 5 m to be consistent with the DEM map. All simulations were calibrated to the runoff flow and runout patterns in the flood and landslide inventory. Calibrations were performed manually by altering related input parameters. All elements (including humans, buildings, and roads) were exposed to a floodwater depth of more than 25 cm and a velocity of more than 2.5 m/s, which are considered to be consistent with flood exposure elements. As the SHALSTAB model can only reveal the occurrence of landslides, blocks that included landslide exposure elements were set to experience landslides during the simulation.

### 5.4 Validation

The difficulty of validating the proposed model lies in its complex components and scarce observations. There is no direct way to assess the final output (city exposure to hazards) of the model. Instead, we used structural validation to check whether each component of the model and its theoretical foundations and underlying assumptions were correct and reasonable (Galán et al., 2009).

The simulation of floods and landslides can be validated using available observation data. HazardCM is designed to support different hazard models, so it does not require the hazard simulation to be flawless. Both the LISFLOOD-FP and SHALSTAB models have been used for years and have been proven to be efficient (see Section 4). Thus, a careful calibration of the hazard simulation using historical data from 2014 was carried out.

In addition, in the ABM, we have followed the basic structure of InaSAFE and the resilience.io model, both were validated by a board of stakeholders and domain experts. The most important output from the ABM is the spatial and temporal population distribution. Despite the difficulty of observing the population distribution for the whole city, the population flow at some vital road junctions can reflect it to some extent. For this reason, the simulated population flow was compared to traffic observations at road junctions.

In fact, this whole exercise highlights the importance of conducting scenario analyses rather than aiming for precise predictions. The aim of our model is to develop a tool to explore critical consequences from the many interrelated complex social processes involved in hazard–human interactions in the context of various alternative futures.

### 5.5 Scenario design

To investigate the interactions between multi-hazards and the city system, different combinations of hazards and city elements were designed as initial conditions of the model. The hazard-related scenarios included hazard type (landslide or flood), hazard magnitude, and hazard timing, as well as location. The rainfall process and its characteristics are of great importance to landslide and flood hazards. Different return periods of rainfall can be used as inputs to produce different hazard magnitudes. The return period of 50 years was used for most demonstrations.

People's daily behaviors are characterized by certain patterns with regard to daily, weekly, monthly, and yearly cycles. The hazard occurrence was configured to happen on a weekday and a weekend. The time of the hazard occurrence was set to 6 am and 6 pm. As disaster response measures adopted by local government are likely to affect people's daily behaviors, both warning and non-warning settings were considered.

**Table 4:** Parameter variations used in the simulation scenarios.

| Scenarios | Hazard type | Rainstorm occurrence time | Human behavior | Weekdays or weekends |
|---|---|---|---|---|
| S1 | Urban flood | 6 am | Daily | Weekdays |
| S2 | Urban flood | 6 am | Daily | Weekends |
| S3 | Urban flood | 6 am | Bad weather | Weekdays |
| S4 | Urban flood | 6 am | Bad weather | Weekends |
| S5 | Urban flood | 6 am | Warning | Weekdays |
| S6 | Urban flood | 6 am | Warning | Weekends |
| S7 | Landslide | 6 am | Daily | Weekdays |
| S8 | Landslide | 6 am | Daily | Weekends |
| S9 | Landslide | 6 am | Bad weather | Weekdays |
| S10 | Landslide | 6 am | Bad weather | Weekends |
| S11 | Landslide | 6 am | Warning | Weekdays |
| S12 | Landslide | 6 am | Warning | Weekends |
| S13 | Urban flood | 6 pm | Daily | Weekdays |
| S14 | Urban flood | 6 pm | Daily | Weekends |
| S15 | Urban flood | 6 pm | Bad weather | Weekdays |
| S16 | Urban flood | 6 pm | Bad weather | Weekends |
| S17 | Urban flood | 6 pm | Warning | Weekdays |

| | | | | |
|---|---|---|---|---|
| S18 | Urban flood | 6 pm | Warning | Weekends |
| S19 | Landslide | 6 pm | Daily | Weekdays |
| S20 | Landslide | 6 pm | Daily | Weekends |
| S21 | Landslide | 6 pm | Bad weather | Weekdays |
| S22 | Landslide | 6 pm | Bad weather | Weekends |
| S23 | Landslide | 6 pm | Warning | Weekdays |
| S24 | Landslide | 6 pm | Warning | Weekends |

Therefore, 24 scenarios covering the above situations were designed in this study (see Table 4). The simulated results according to different hazard, human, and city scenarios are given in Section 5.6-5.8. It is worth noting that only part of these scenarios are discussed and displayed due to space limitations, but the model can manage all the mentioned scenarios.

### 5.6 Spatial and temporal distribution simulation of the population

The population activities were simulated in a day for three scenarios—daily (no disaster), bad weather (rainstorm), and warning (rainstorm and warning)—and considered the difference in population activities between weekdays and weekends. The model output the simulation results every 30 minutes, organized in blocks. The spatial resolution could be adapted to the study area, and in this case, the smallest block area was 391 $m^2$.

Figures 7 illustrates the population distribution among the six scenarios, respectively. At 9 o'clock, there were many people in the center (business blocks) on the weekday and in the northeast (recreational blocks) on the weekend. Seen from the entire area, the population distribution on the weekday was more uniform than that on the weekend. Moreover, the three scenarios on the weekend were quite different from each other, while differences among the weekdays were not obvious. The reason is that people are more likely to cancel recreational activities than work, so the population during the weekend bad weather and warning scenarios differed significantly from the population during daily scenarios. The population trends of different blocks and roads are shown in Figure 8. Figure 8(a) indicates that, among the three weekend scenarios, the population in the recreational area (Block 77) changed more than the population in the business area (Block 113) among the three weekday scenarios.

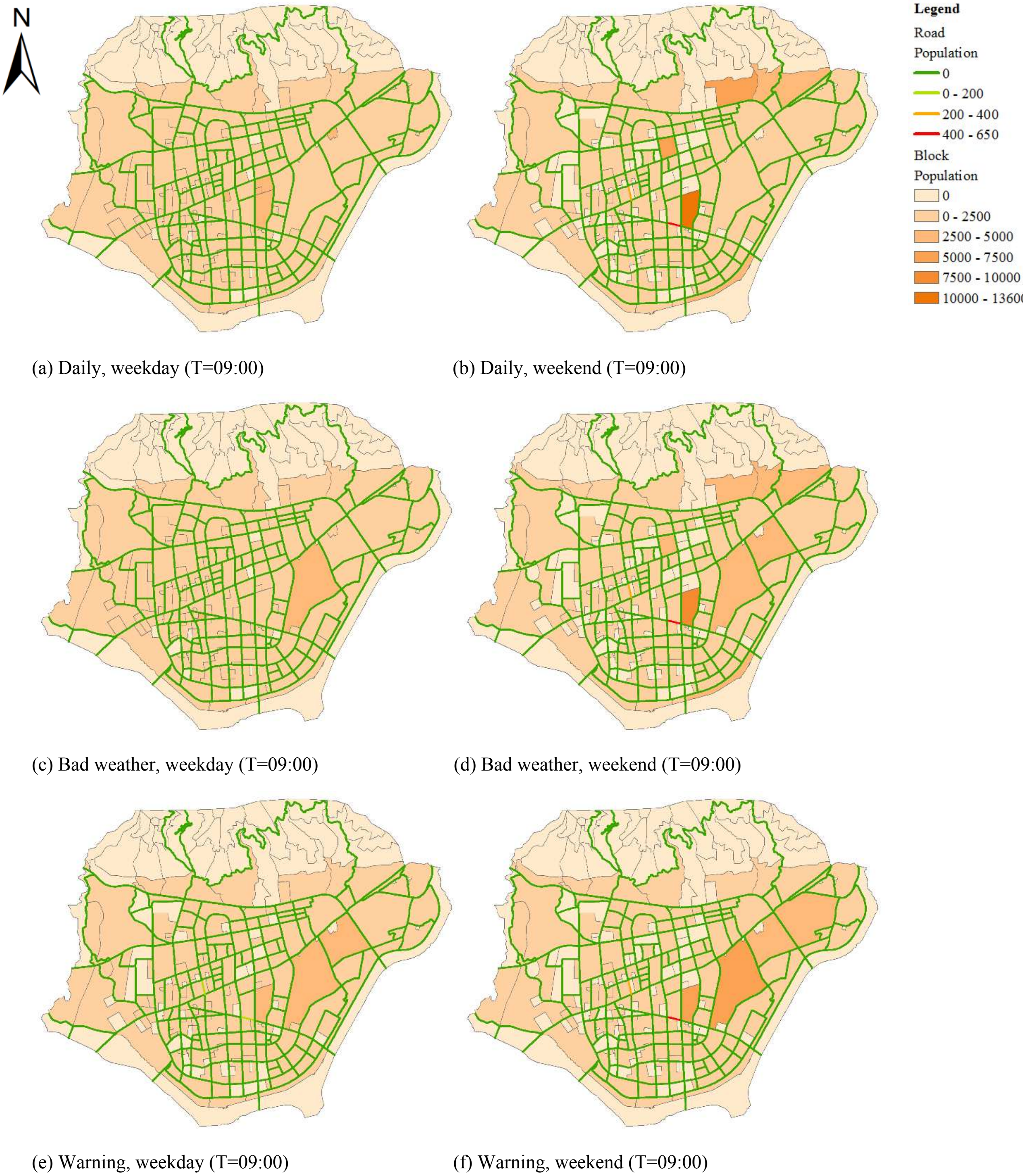


(a) Daily, weekday (T=09:00) (b) Daily, weekend (T=09:00)

(c) Bad weather, weekday (T=09:00) (d) Bad weather, weekend (T=09:00)

(e) Warning, weekday (T=09:00) (f) Warning, weekend (T=09:00)

Figure 7. Map of population distribution.

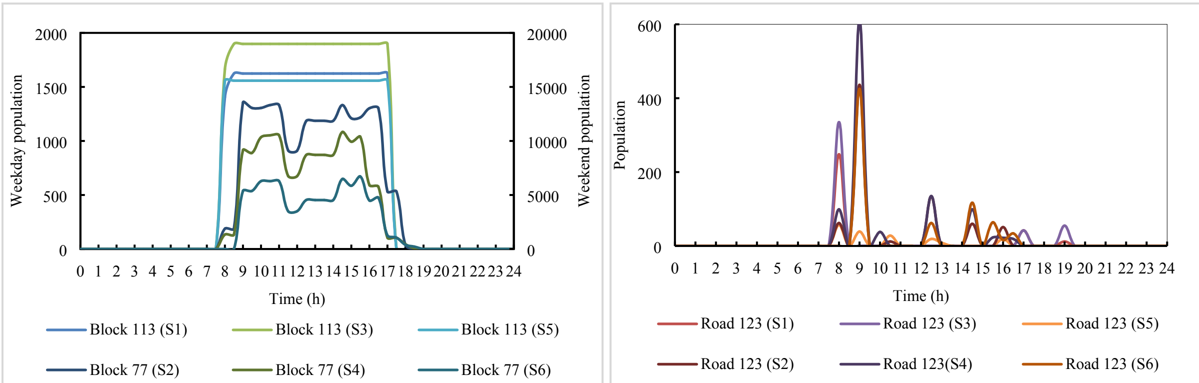


(a) Block population (b) Road population

Figure 8. Changes of population with time. S1-6 mean six flood scenarios as shown in Table 4.

The reliability of the simulation of the spatiotemporal population distribution was indirectly verified by using traffic flow data. The simulated total number of residents passing through the four intersections (such as the junction of the Liqing and Huayuan roads) and the actual measured traffic flow (multi-day average results) at the intersections during the morning and evening peak hours on weekdays and weekends are shown in Fig. 9. Real means measured value. LQ is Liqing Road, KF is Kaifa Road, HY is Huayuan Road, ZJ is Zijin Road, and LT is Lutang Street. It can be seen that the simulated and measured values were similar.

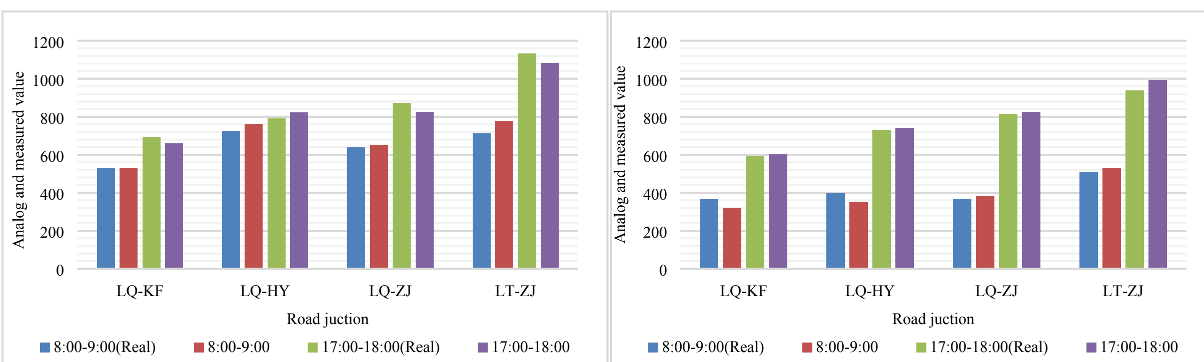


(a) Weekday (b) Weekend

Figure 9. Traffic flow and population simulation results during peak hours on weekdays and weekends.

### 5.7 Urban flood and landslide simulation results

The Chicago hyetograph method's (CHM) rainstorm intensity formula was used to design a rainstorm with a 50-year return period in the study area. The rainfall duration lasted six hours (6 am to 12 pm for S1-6, and 6 pm to 12 am for S13-24), and the cumulative rainfall was about 148.59

mm. The CHM parameters referenced the rainstorm intensity formula of Lishui City in the "Zhejiang City Rainstorm Intensity Formula Table" published by the Hangzhou Planning Bureau of Zhejiang Province, as in Equation (5):

$$i = \frac{1265.3(1 + 0.587 \times \lg 50)}{167(t + 5.919)^{0.611}} \tag{5}$$

where $i$ is the rainfall intensity (mm/min) and $t$ is the time. Based on the rainfall simulation results, this study used the LISFLOOD-FP model to simulate the flood process in the city. The model output the simulation results (using grids with 5 m resolution) every 30 minutes. The water depth and velocity results of the flooding were extracted according to the block, and the maximum value was taken considering the block integrity. Figure 8 shows the changes in the accumulated flooded block area in terms of differences in water depth and velocity, reflecting the dynamic characteristics of the flood process and its impact on the study area. According to Figure 10 (a), many blocks were flooded, and the water depth exceeded the exposure threshold. As the rainfall ended, the flooding in most blocks subsided, while the flooding in a few blocks was more serious. Additionally, as seen in Figure 10 (b), the water velocity of a few blocks overtook the exposure threshold at a later stage of the rainfall (2 - 6 hours).

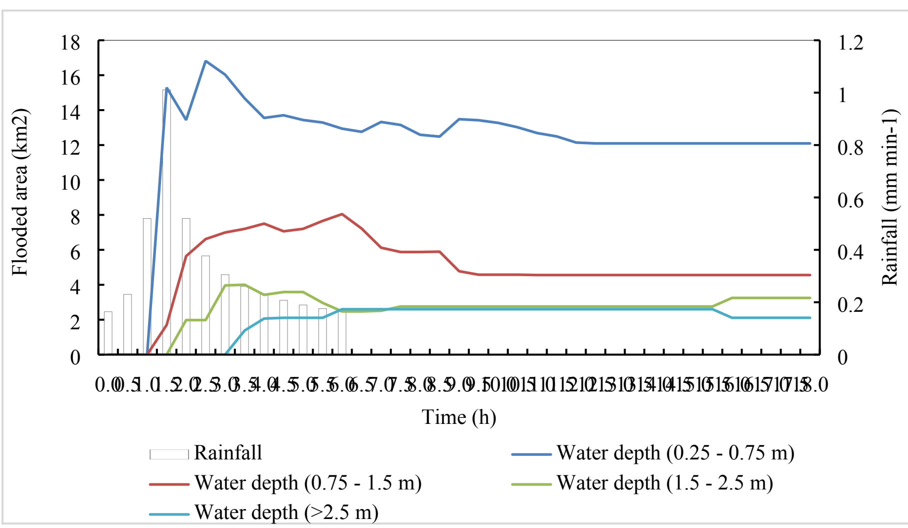


(a)

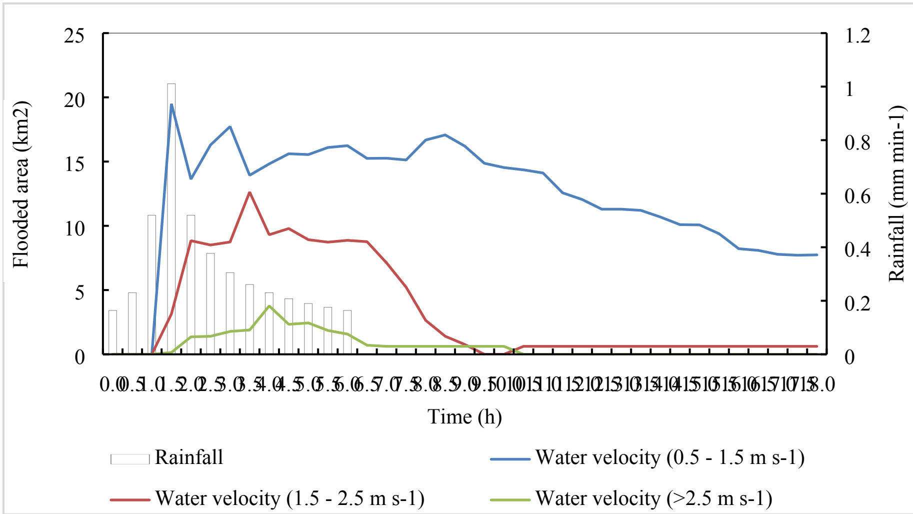


(b)

Figure 10. Changes of flooded area in different time steps.

The r.shalstab model was used to determine the study area's susceptibility to landslides. Time and spatial resolutions of landslide susceptibility were the same as those of the flood simulation results. The rainfall data we used were the same as the simulation data used in the above flood simulation. The block with a susceptibility value between 1 and 4 would be exposed to landslides. The landslide susceptibility results according to the block are as shown in Figure 11, which corresponds to 6 am, when the rain started. Figure 12 shows the block area with different susceptibility at different times. It can be seen that the area of the unconditionally unstable block remained stable, while the others slightly rose or declined during the rainfall period because of the water velocity change.

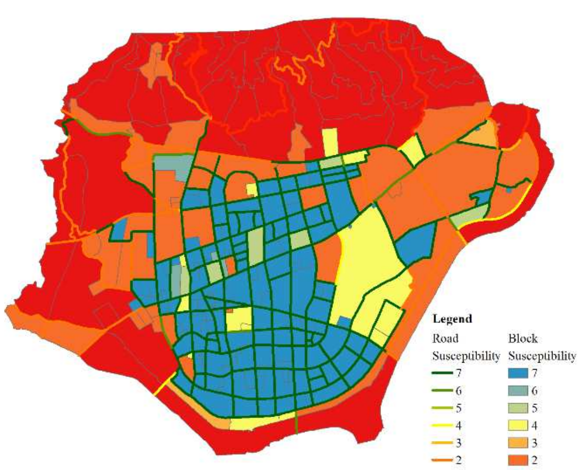


Figure 11. Map of landslide susceptibility.

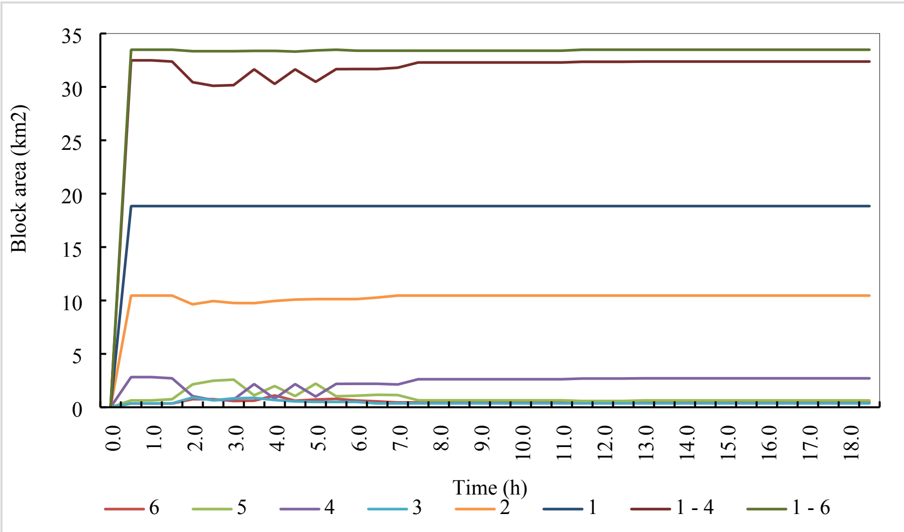


Figure 12. The area of blocks with different landslide susceptibility in different time steps.

### 5.8 City dynamic exposure to hazard events

The exposure of roads and buildings to flooding and landslides were represented by exposed road length and building area, respectively. They were determined by coupling the two results described above, including the simulation results of the hazard and population distribution. Figure 13 indicates the exposure of the road and building to flooding and landslides at 12 pm, when the rain (6 am to 12 pm) ended. In terms of their distribution, the southern part of the study area was more exposed to floods, while the northern areas were more susceptible to landslides, which is consistent with the topography of the study area.

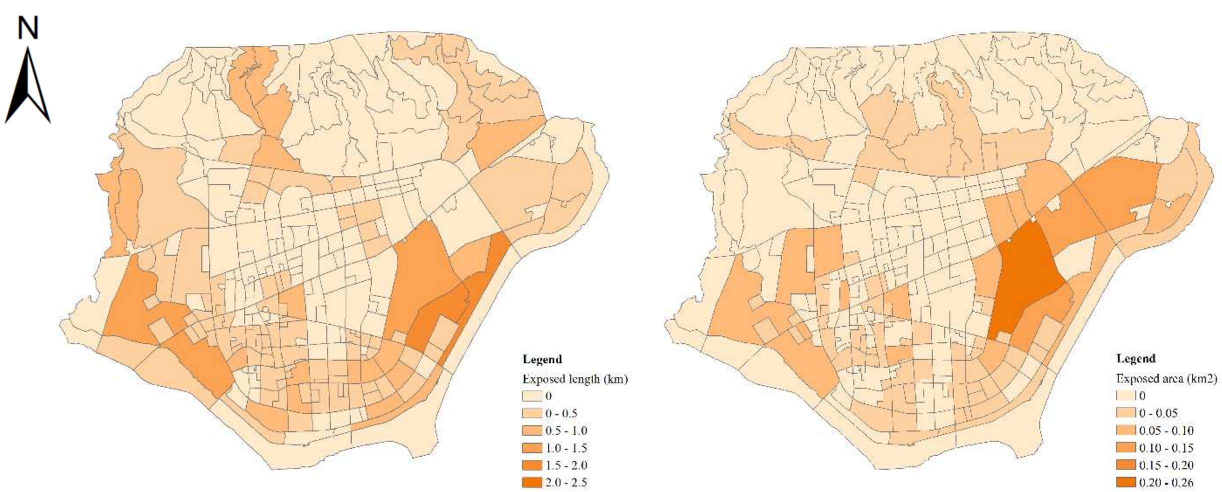


(a) Road exposure (Flood, T=12:00) (b) Building exposure (Flood, T=12:00)

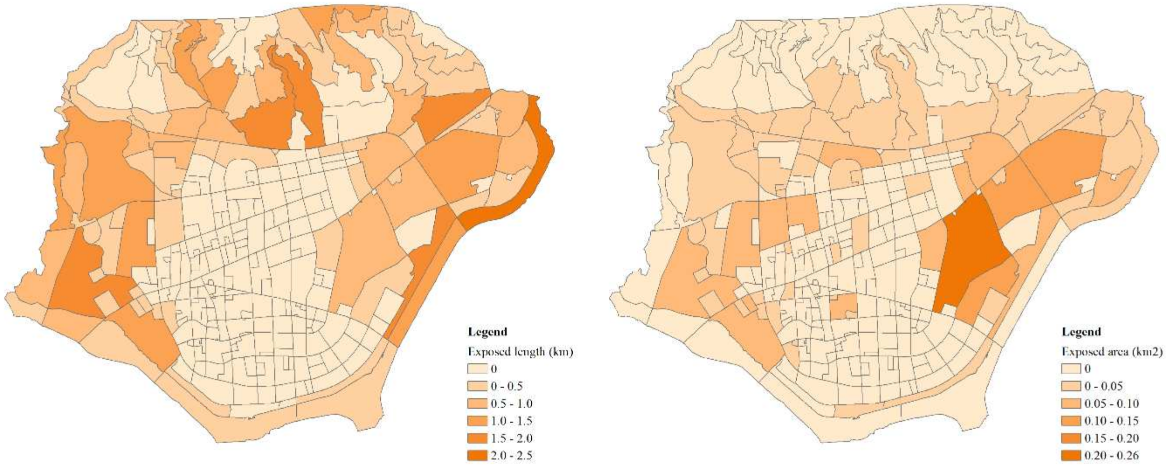


(c) Road exposure (Landslide, T=12:00) (d) Building exposure (Landslide, T=12:00)

Figure 13. Map of road exposure and building exposure to flood and landslide (rainstorm during 6 am to 12 pm).

The changes in road and building exposure in the study area are shown in Figure 14. It can be found that the exposure to the flood changed greatly, while that of the landslide remained basically unchanged. And the landslide posed a greater threat to the road than the flood; while for the building, the maximum exposed building area during flooding was more than twice that of the landslide.

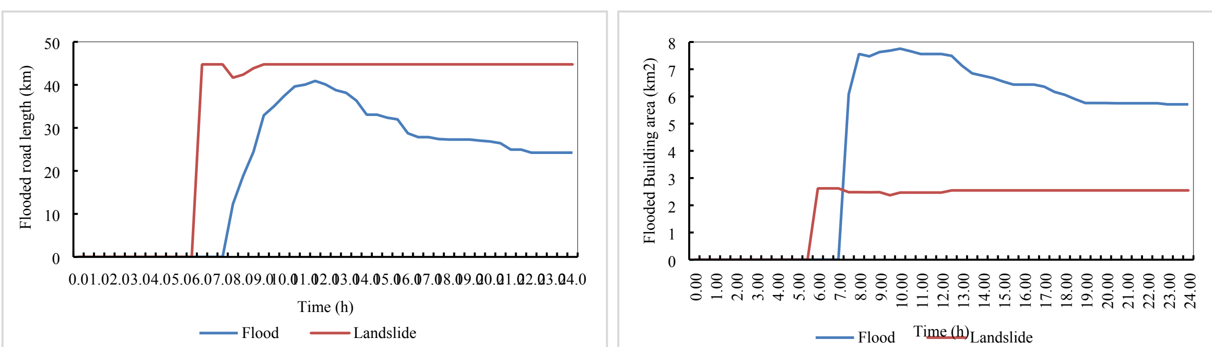


(a) Road exposure (b) Building exposure

Figure 14. Changes in road and building exposures (rainstorm during 6 am to 12 pm).

Changes regarding total population exposure of all blocks in different scenarios are shown in Figure 15, which demonstrates that the population exposure was dynamic. Specifically, the exposed population to floods increased rapidly with the accumulation of water, and then fluctuated and finally remained stable (Figure 15 (a)). As for the population exposure to landslides (Figure 15 (b)), the number rose to the maximum immediately at the beginning of rainfall. After two hours, it decreased with the movement of population and remained stable until 17 pm, and then went up to the same maximum as before and remained stable. Compared with floods, landslides posed a greater threat to the population of the study area. In Figure 15 (c), exposed population at night was similar among different scenarios due to stable population distribution, and changed with flood. For landslides in Figure 15 (d), exposed population remained stable during night which was the results of stable susceptibility and population distribution. In addition, it was obvious that population exposed to flood which happened at night was much larger than that in the day.

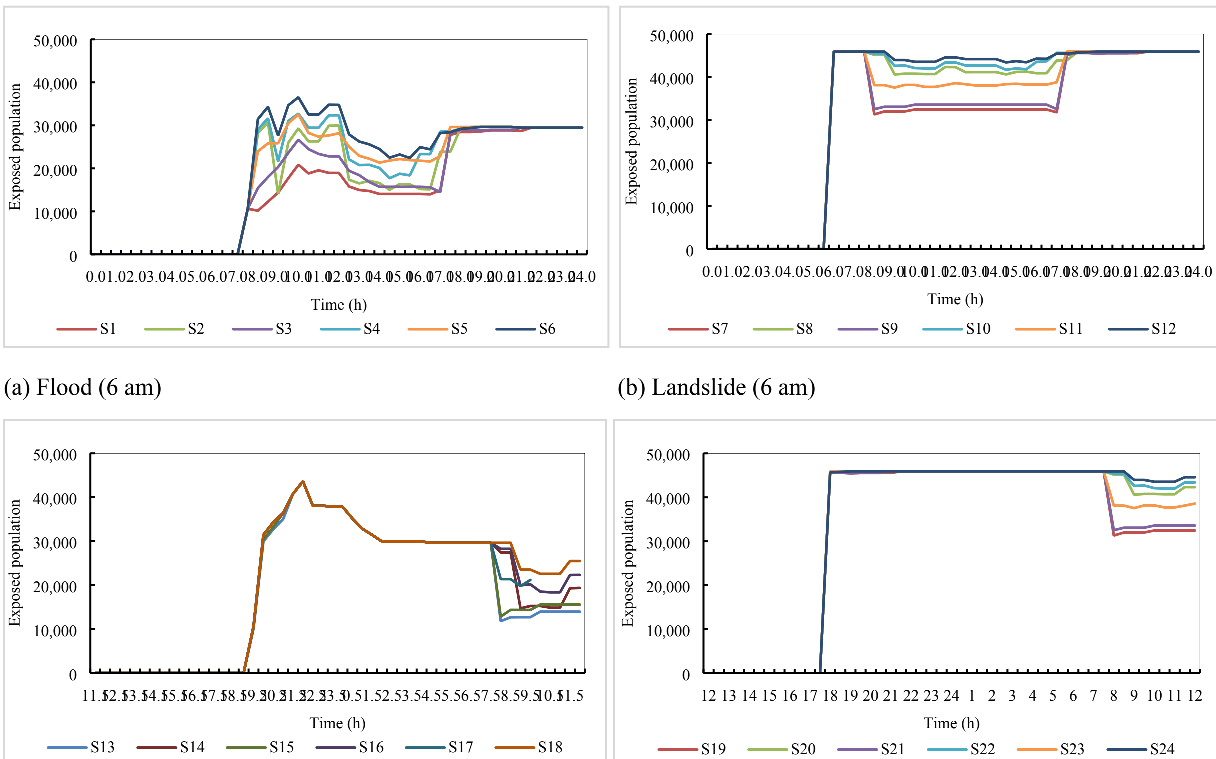


(a) Flood (6 am) (b) Landslide (6 am)

(c) Flood (6 pm) (d) Landslide (6 pm)

Figure 15. Changes in the population exposure for the 24 scenarios.

## 6. Discussion

HazardCM was based on the assumption that there is no migration into and out of the city. Therefore the mobility of population spatial and temporal distribution simulation results was smaller than the actual situation, which caused uncertainty of the results of population exposure. Although the number of migrants in the urban area during daytime is large owing to its geographical location, it is difficult to set up daily routine maps for such people. So far, we have not obtained related data and information about the percentage of this type of population and their movements in the study area. We will consider adding this type of people when we have enough data to set up their daily routine maps in the future.

As we considered people's responses to disasters, we noted that different choices of activities were available to them in each scenario, resulting in different exposure levels for the population at the same time. The exposed population to floods and landslides in the warning scenario was the greatest among daily, bad weather, and warning scenarios. The reason is that this study assumed that the disaster response behavior adopted by residents corresponds to reduction in travel, that is, the residents directly choose their residential area as shelters but not based on the exposure level of the residential area. Therefore, when a residential area was exposed to a landslide, the residents chose to reduce travel in the disaster scenario, resulting in an increase in the population of the residential area, and thereby increasing the exposed population.

By coupling the simulation of different disaster scenarios, including different disaster type and occurrence time, with different scenarios of population activities, we can obtain the spatial distribution and change process of road, building, and population exposure in the region. High-resolution and quantitative results can support policy makers and minimize casualties and damage to roads and buildings.

Based on HazardCM, we only designed 24 scenarios to investigate dynamic exposure of different hazard type (urban flood and landslide), hazard occurrence time (day and night), human behavior (daily, bad weather, and warning), and weekdays or weekends. The intensity of a rainstorm (or flood / landslide) cause different impacts on a city system. We had made some attempts in this aspect which not included in this paper. For example, Zhu et. al. (2018) investigated the influence of urban flooding on traffic congestion, with diverse rainfall return periods and various durations of flood occurrence.

## 7. Conclusion

This study proposed a human–hazard coupled platform for calculating accurate spatiotemporal DYE in the context of different types of natural hazards. The platform includes the following key components: 1) an urban environment module that provides an analysis framework and spatial expression of city elements, including buildings and networks; 2) an ABM module that includes a human activity model and human adaptation in a hazard environment; 3) a hazard coupled module that connects hazards to human activity within the urban environment through an external or internal coupler; and 4) an assessment module that estimates the DYE of natural hazards. The rainfall-triggered natural hazards (flood and landslides) during extreme hydrometeorological events were modeled, and their DYE was investigated in a typical city in China. Compared with a traditional exposure estimation model such as InaSAFE, which assumes the exposure elements are static and ignores the interactions among these elements, this model offers a way to investigate the space–time characteristics of exposure while considering the dynamic nature of both humans and hazards.

As natural hazards and cities are regarded as systems of systems, modeling them with special consideration for the integration between them is extremely complicated. The proposed platform certainly has limitations in reflecting all details within the human–hazard environment. For example, there are a number of parameters such as hazard exposure threshold that are determined subjectively, which may introduce uncertainty to the final outcomes. The validation of the hazard simulation and exposure calculation was not investigated completely in this study, as some observed data were difficult to obtain. Nevertheless, the proposed model can improve our understanding of hazard–human interactions in a united platform and support stakeholder decision-making in risk management of natural hazards. More natural hazards will be included in future research, and integrated modeling of multi-hazards will also be investigated. The model will be published as open source in the near future. It is expected the proposed model can be applied in other cities with different hazards and urban environments.

## Acknowledgments

This work was supported by the National Natural Science Foundation of China (Nos: 41871299, 41771424, and 41631175), the Newton Fund via the Natural Environment Research Council (NERC), and the Economic and Social Research Council (ESRC) (NE/N012143/1). The authors acknowledge Zaihui Chen and Lijun Jiang in the Bureau of Surveying and Mapping of Lishui and Peng Wu in the Lishui Hydrological Station for their efforts in providing and pre-processing data.

## References

Abebe, Y.A., Ghorbani, A., Nikolic, I., Vojinovic, Z., Sanchez, A., 2019. A coupled flood-agent-institution modelling (CLAIM) framework for urban flood risk management. Environmental Modelling & Software 111 483-492.

Aerts, J.C.J.H., Botzen, W.J., Clarke, K.C., Cutter S. L., Hall J. W., Merz B., Michel-Kerjan E., Mysiak J., Surminski. S., Kunreuther H., 2018. Integrating human behaviour dynamics into flood disaster risk assessment. Nature Clim Change 8 193–199.

Arentze, T., Timmermans, H., 2000. Albatross: a learning based transportation oriented simulation system. Citeseer.

Atun, F., 2014. Understanding effects of complexity in cities during disasters, Understanding complex urban systems: multidisciplinary approaches to modeling. Springer, pp. 51-65.

Auld, J., Mohammadian, A.K., 2012. Activity planning processes in the Agent-based Dynamic Activity Planning and Travel Scheduling (ADAPTS) model. Transportation Research Part A: Policy Practice 46(8) 1386-1403.

Balmer, M., Axhausen, K.W., Nagel, K., 2006. Agent-based demand-modeling framework for large-scale microsimulations. Transportation Research Record 1985(1) 125-134.

Bates, P., Trigg, M., Neal, J., Dabrowa, A., 2013. LISFLOOD-FP User manual.

Bates, P.D., De Roo, A., 2000. A simple raster-based model for flood inundation simulation. Journal of hydrology 236(1-2) 54-77.

Behzadian, K., Kapelan, Z., Govindarajan, V., Brattebø, H., Sægrov, S., 2014. WaterMet2: a tool for integrated analysis of sustainability-based performance of urban water systems. Drinking Water Engineering and Science.

Bhat, C., Guo, J., Srinivasan, S., Sivakumar, A., 2004. A comprehensive econometric micro-simulator for daily activity-travel pattern (CEMDAP), EIRASS workshop on Progress in activity-based analysis, Maastricht, The Netherlands.

Bhat, C.R., Koppelman, F.S., 1999. Activity-based modeling of travel demand, Handbook of transportation Science. Springer, pp. 35-61.

Bisht, D.S., Chatterjee, C., Kalakoti, S., Upadhyay, P., Sahoo, M., Panda, A., 2016. Modeling urban floods and drainage using SWMM and MIKE URBAN: a case study. Natural Hazards 84(2) 749-776.

Budimir, M., Atkinson, P., Lewis, H., 2014. Earthquake-and-landslide events are associated with more fatalities than earthquakes alone. Natural Hazards 72(2) 895-914.

Burton, A., Bathurst, J., 1998. Physically based modelling of shallow landslide sediment yield at a catchment scale. Environmental Geology 35(2-3) 89-99.

Cho, S.Y., Chang, H., 2017. Recent research approaches to urban flood vulnerability, 2006–2016. Natural Hazards 88(1) 633-649.

Coulthard, T.J., Neal, J.C., Bates, P.D., Ramirez, J., de Almeida, G.A., Hancock, G.R., 2013. Integrating the LISFLOOD‐FP 2D hydrodynamic model with the CAESAR model: implications for modelling landscape evolution. Earth Surface Processes Landforms 38(15) 1897-1906.

David, J.Y., Sangwan, N., Sung, K., Chen, X., Merwade, V., 2017. Incorporating institutions and collective action into a sociohydrological model of flood resilience. Water Resources Research 53(2) 1336-1353.

Dawson, R.J., Peppe, R., Wang, M., 2011. An agent-based model for risk-based flood incident management. Natural Hazards 59(1) 167-189.

de Moel, H., Aerts, J.C., Koomen, E., 2011. Development of flood exposure in the Netherlands during the 20th and 21st century. Global Environmental Change 21(2) 620-627.

Dietrich, W., Montgomery, D., 1998. SHALSTAB: A digital terrain model for mapping shallow landslide potential. National Council of the Paper Industry for Air and Stream Improvement. Technical Report.

du Plessis A., 2019 Climate Change: Current Drivers, Observations and Impacts on the Globe's Natural and Human Systems. In: Water as an Inescapable Risk. Springer Water. Springer, Cham

Figueiredo, R., Schröter, K., Weiss-Motz, A., Martina, M.L., Kreibich, H., 2018. Multi-model ensembles for assessment of flood losses and associated uncertainty. Natural Hazards & Earth System Sciences 18(5) 1297-1314.

Galán, J.M., López‐Paredes, A., Del Olmo, R., 2009. An agent‐based model for domestic water management in Valladolid metropolitan area. Water Resources Research 45(5).

Gamow, G., 1970. My world line: An informal autobiography. Viking Press, New York.

Garcia, R.A., Oliveira, S., Zêzere, J., 2016. Assessing population exposure for landslide risk analysis using dasymetric cartography. Natural Hazards & Earth System Sciences 16(12) 2769-2782.

Gärling, T., Kwan, M.-p., Golledge, R.G., 1994. Computational-process modelling of household activity scheduling. Transportation Research Part B: Methodological 28(5) 355-364.

Gill, J.C., Malamud, B.D., 2014. Reviewing and visualizing the interactions of natural hazards. Earth-Science Reviews 52(4) 680-722.

Gill, J.C., Malamud, B.D., 2017. Anthropogenic processes, natural hazards, and interactions in a multi-hazard framework. Earth-Science Reviews 166 246-269.

Gironás, J., Roesner, L.A., Rossman, L.A., Davis, J., 2010. A new applications manual for the Storm Water Management Model (SWMM). Environmental Modelling & Software 25(6) 813-814.

Gorsevski, P.V., Gessler, P.E., Boll, J., Elliot, W.J., Foltz, R.B., 2006. Spatially and temporally distributed modeling of landslide susceptibility. Geomorphology 80(3-4) 178-198.

Grahn, T., Nyberg, L., 2017. Assessment of pluvial flood exposure and vulnerability of residential areas. International Journal of Disaster Risk Reduction 21 367-375.

Güneralp, B., Güneralp, İ., Liu, Y., 2015. Changing global patterns of urban exposure to flood and drought hazards. Global Environmental Change 31 217-225.

Hagberg, A., Swart, P., S Chult, D., 2008. Exploring network structure, dynamics, and function using NetworkX. Los Alamos National Lab.(LANL), Los Alamos, NM (United States).

House‐Peters, L.A., Chang, H., 2011. Urban water demand modeling: Review of concepts, methods, and organizing principles. Water Resources Research 47(5).

Hsu, W.-K., Chiang, W.-L., Xue, Q., Hung, D.-M., Huang, P.-C., Chen, C.-W., Tsai, C.-H., 2013. A probabilistic approach for earthquake risk assessment based on an engineering insurance portfolio. Natural Hazards 65(3) 1559-1571.

Ivy-Ochs, S., Poschinger, A., Synal, H.-A., Maisch, M., 2009. Surface exposure dating of the Flims landslide, Graubünden, Switzerland. Geomorphology 103(1) 104-112.

Javanmardi, M., Langerudi, M.F., Shabanpour, R., Mohammadian, A., 2016. An optimization approach to resolve activity scheduling conflicts in ADAPTS activity-based model. Transportation 43(6) 1023-1039.

Jongman, B., Koks, E.E., Husby, T.G., Ward, P.J., 2014. Increasing flood exposure in the Netherlands: implications for risk financing. Natural Hazards & Earth System Sciences 14(5) 1245-1255.

Kappes, M.S., Keiler, M., von Elverfeldt, K., Glade, T., 2012a. Challenges of analyzing multi-hazard risk: a review. Natural Hazards 64(2) 1925-1958.

Kappes, M.S., Papathoma-Koehle, M., Keiler, M., 2012b. Assessing physical vulnerability for multi-hazards using an indicator-based methodology. Applied Geography 32(2) 577-590.

Lant, J., Durand, M., Andreadis, K., Alsdorf, D., 2010. A hydraulic modeling framework for producing urban flooding maps in Zanesville, Ohio. In Watershed Management 2010: Innovations in Watershed Management under Land Use and Climate Change 248-257.Li, J., Li, Y., Li, Y., 2016. SWMM-based evaluation of the effect of rain gardens on urbanized areas. Environmental Earth Sciences 75(1) 17.

Li, Z., Dong, W., 2010. A stroke-based method for automated generation of schematic network maps. International Journal of Geographical Information Science 24(11) 1631-1647.

Lindell, M.K., Perry, R.W., 2003. Communicating environmental risk in multiethnic communities. Sage Publications.

McNally, M.G., 1996. An activity-based microsimulation model for travel demand forecasting.

Mignan, A., Wiemer, S., Giardini, D., 2014. The quantification of low-probability–high-consequences events: part I. A generic multi-risk approach. Natural Hazards 73(3) 1999-2022.

Miller, E.J., Roorda, M.J., 2003. Prototype model of household activity-travel scheduling. Transportation Research Record 1831(1) 114-121.

Montgomery, D.R., Dietrich, W.E., 1994. A physically based model for the topographic control on shallow landsliding. Water Resources Research 30(4) 1153-1171.

Montz, B.E., Tobin, G.A., Hagelman, R.R., 2017. Natural hazards: explanation and integration. Guilford Publications.

NetLogo, 2018. The NetLogo 6.0.4 User Manual.

O'loughlin, E., 1986. Prediction of surface saturation zones in natural catchments by topographic analysis. Water Resources Research 22(5) 794-804.

Ozdemir, H., Sampson, C. C., De Almeida, G. A. M., Bates, P. D., 2013. Evaluating scale and roughness effects in urban flood modelling using terrestrial lidar data. Hydrology and Earth System Sciences 17(10) 4015-4030.

Park, Y.M., Kwan, M.-P., 2017. Individual exposure estimates may be erroneous when spatiotemporal variability of air pollution and human mobility are ignored. Health Place 43 85-94.

Pellicani, R., Van Westen, C.J., Spilotro, G., 2014. Assessing landslide exposure in areas with limited landslide information. Landslides 11(3) 463-480.

Pittore, M., Wieland, M., Fleming, K., 2014. Perspectives of a global, dynamic Exposure Model for Geo-Risk Assessment from Remote Sensing to Crowd-Sourcing. Global Assessment Report on Disaster Risk Reduction.

Porta, S., Crucitti, P., Latora, V., 2006. The network analysis of urban streets: a primal approach. Environment Planning B: planning design 33(5) 705-725.

Project, I., 2014. InaSAFE documentation.

Promper, C., Gassner, C., Glade, T., 2015. Spatiotemporal patterns of landslide exposure–a step within future landslide risk analysis on a regional scale applied in Waidhofen/Ybbs Austria. International Journal of Disaster Risk Reduction 12 25-33.

QGIS, 2018. QGIS.

Rasouli, S., Timmermans, H., 2014. Activity-based models of travel demand: promises, progress and prospects. International Journal of Urban Sciences 18(1) 31-60.

Recker, W.W., 1995. The household activity pattern problem: general formulation and solution. Transportation Research Part B: Methodological 29(1) 61-77.

RepastCity, 2012. RepastCity - A demo virtual city (version 3).

Riddell, G. A., van Delden, H., Maier, H. R., Zecchin, A. C., 2019. Exploratory scenario analysis for disaster risk reduction: Considering alternative pathways in disaster risk assessment. International Journal of Disaster Risk Reduction 39 101230.

Ruin, I., Lutoff, C., Boudevillain, B., Creutin, J.-D., Anquetin, S., Rojo, M.B., Boissier, L., Bonnifait, L., Borga, M., Colbeau-Justin, L., 2014. Social and hydrological responses to extreme precipitations: an interdisciplinary strategy for postflood investigation. Weather, climate, society 6(1) 135-153.

Shabou, S., Ruin, I., Lutoff, C., Debionne, S., Anquetin, S., Creutin, J.-D., Beaufils, X., 2017. MobRISK: a model for assessing the exposure of road users to flash flood events. Natural Hazards & Earth System Sciences 17(9) 1631.

Simphony, R., 2016. Repast Simphony Project.

Smith, L., Beckman, R., Baggerly, K., 1995. TRANSIMS: Transportation analysis and simulation system. Los Alamos National Lab., NM (United States).

Sun, N., Hong, B., Hall, M., 2014. Assessment of the SWMM model uncertainties within the generalized likelihood uncertainty estimation (GLUE) framework for a high‐resolution urban sewershed. Hydrological processes 28(6) 3018-3034.

Terti, G., Ruin, I., Anquetin, S., Gourley, J.J., 2015. Dynamic vulnerability factors for impact-based flash flood prediction. Natural Hazards 79(3) 1481-1497.

Triantafyllidis, C.P., Koppelaar, R.H., Wang, X., van Dam, K.H., Shah, N., 2018. An integrated optimisation platform for sustainable resource and infrastructure planning. Environmental Modelling & Software 101 146-168.

West, D.B., 1996. Introduction to graph theory. Prentice hall Upper Saddle River, NJ.

Wood, M., Hostache, R., Neal, J., Wagener, T., Giustarini, L., Chini, M., Corato, G., Matgen, P., Bates, P., 2016. Calibration of channel depth and friction parameters in the LISFLOOD-FP hydraulic model using medium-resolution SAR data and identifiability techniques. Hydrology & Earth System Sciences 20(12) 4983-4997.

YAML, 2017. YAML.

Zhu, J., Dai, Q., Deng, Y., Zhang, A., Zhang, Y., Zhang, S., 2018. Indirect damage of urban flooding: Investigation of flood-induced traffic congestion using dynamic modeling. Water 10(5) 622.